Bachir BOUMEDIENE[1], Attalah SMAILI[1], Tayeb ALLAOUI[1], Abderrahmane BERKANI[1], Fabrizio MARIGNETTI[2]

Laboratory of L2GEGI, Department of Electrical Engineering, University of Tiaret, Algeria (1)
Dipartimento di Automazione Università degli Studi di Cassino, Italy (2)

doi:10.15199/48.2021.03.04

Backstepping Control Strategy for Multi-source Energy System based Flying capacitor Inverter and PMSG

Abstract. *In this paper, renewable photovoltaic (PV) and wind turbine (WT) generators with battery are coupled via a flying capacitor inverter to a power grid in parallel with an alternating load. This paper studies a new control structure focused a backstepping control of the energy storage system. The proposed methods to adjust the active and reactive power by adjusting the currents, the DC bus voltage on the grid side converter, as well as the battery voltage allow three selective control targets to be achieved, the objective is to obtain purely sinusoidal signals and symmetrical gate current, suppresses reactive power ripples and cancels active power ripples in the event of grid imbalance. In order to optimize the power flow in the different parts of the production process, an energy management algorithm is developed in order to mitigate the fluctuations of the load, the considered multi-sources on-grid system was implemented in the Matlab/Simulink, the results show the effectiveness of the proposed method. To analyze our approach, a prototype is modeled, simulated and can be realized in an experimental test setup.*

Streszczenie. *W tym artykule odnawialne generatory fotowoltaiczne (PV) i turbiny wiatrowe (WT) z baterią są sprzężone za pośrednictwem falownika ze swobodnym kondensatorem z siecią energetyczną równolegle ze zmiennym obciążeniem. Przeanalizowano nową strukturę controli sterowania, która skupiła się na wstecznej kontroli systemu magazynowania energii. Proponowane metody regulacji mocy czynnej i biernej poprzez regulację prądów, napięcia szyny DC po stronie sieciowej oraz napięcia akumulatora pozwalają na osiągnięcie trzech celów regulacji selektywnej, celem jest uzyskanie sygnałów czysto sinusoidalnych i symetrycznych. prąd bramki, tłumi tętnienia mocy biernej i anuluje tętnienia mocy czynnej w przypadku braku równowagi sieci. W celu optymalizacji przepływu mocy w różnych częściach procesu produkcyjnego opracowano algorytm zarządzania energią w celu złagodzenia wahań obciążenia, rozważany wielozródłowy system on-grid został zaimplementowany w programie Matlab / Simulink, wyniki pokazują skuteczność proponowanej metody. Aby przeanalizować nasze podejście, modeluje się prototyp, przeprowadza symulację i może zostać zrealizowany w eksperymentalnej konfiguracji testowej. (**Wsteczna kontrola systemu energetycznego z wieloma różnymi źródłami wykorzzystująca falownik i algorytm PMSD**)*

Keywords: PMSG, Flying Capacitor Multilevel Inverter, Multi-source System, Backstepping Control, Battery, Power Management.
Słowa kluczowe: PMSG, falownik wielopoziomowy z kondensatorem latającym, system z wieloma źródłami, kontrola wsteczna,.

Introduction

Renewable energy has emerged as a viable option for contributing to electric power supply in developing countries due to continuing technological advancements, cost deductions and increase in energy demand. Solar and wind energies are the most attractive substitutes to fossil fuels since these are inexhaustible, freely available, cost effective and pollution free. These systems usually exploit the coupling between photovoltaic (PV) and wind generators but can also be coupled to conventional generators such as diesel generators [1], fuel cells, hydrogen storage, and batteries [2]. In this paper, a hybrid on-grid supply system including PV and wind generators with battery storage is studied for producing electricity [3, 4].

The Flying Capacitor Multilevel Inverter, have many attractive properties for medium voltage applications including, in particular, the advantage of transformer-less operation and the ability to naturally maintain the flying capacitors voltages at their target operating levels [5]. Furthermore, the main future of this configuration is making possible to share the voltage constraint on several switches; so the voltage ratings of capacitors and the semiconductor losses are reduced. In such devices, the use of a Power Management System (PMS) is of prime importance for optimal operation and represents a key element of the system. Many alternative power management strategies can be used to manage an on-grid hybrid energy system [6].

The rest of the paper is organized as follows: physical modelings of different part of the study system with their equations model are shown in section 2. The modeling and control of flying capacitor inverter is set in section 3.

in section 4, the system configuration is defined and the models of components employed for each subsystem are described. Section 5 described the backstepping controller of current and DC voltage. Section 6 shows the principle of the voltage capacitor balancing control of flying capacitor inverter. The simulations results of the studied are presented in section 7. Finally, conclusions are drawn in section 8.

Advanced Modeling of System Components

Wind energy system

Wind Turbine

The wind generator consists of a wing which captures the kinetic energy of the wind coupled directly with a synchronous generator which delivers on a DC bus via a diode rectifier; this is the retained structure for this modeling and simulation work. The Fig. 1 show the block diagram of the wind turbine.

The mechanical power of a wind turbine is expressed as follows [7]:

$$P_{mec} = \frac{1}{2}\rho A C_P V_W^3 = C_p P_W \tag{1}$$

The ratio λ, called the tip speed ratio, is give:

$$\lambda = \frac{\omega_W R_r}{V_W} \tag{2}$$

The power coefficient C_p can be written as:

$$C_p(\lambda,\beta) = 0.5\left(116\frac{1}{\lambda_i} - 0.4\beta - 5\right)e^{-\frac{21}{\lambda_i}} \tag{3}$$

with: $\frac{1}{\lambda_i} = \frac{1}{\lambda + 0.08\beta} - \frac{0.035}{1+\beta^3}$

The torque wind can expressed as:

$$T_W = T_{mec} = \frac{1}{2}\frac{C_P \rho R A V_W^2}{\lambda} \tag{4}$$

It should be noted that the mechanical torque transmitted to the generator is the same as the aerodynamics torque, since there is no gearbox.

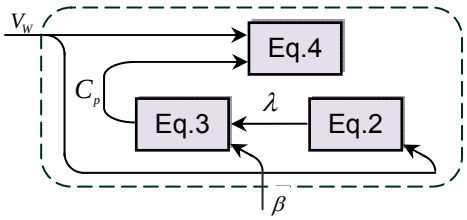

Fig. 1. Bloc diagram of wind turbine

Fig.2 represents the transmitted power according to the rotor PMSG speed for various values of the wind speed.

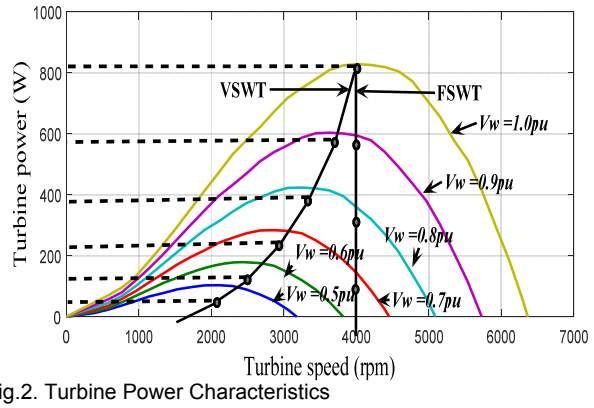

Fig.2. Turbine Power Characteristics

Permanent Magnet Synchronous Generator Model

The permanent magnet synchronous generator model used is modeled by the following equations [8]:

$$v_{sd} = R_s i_{sd} + L_d \frac{di_{sd}}{dt} - \omega_e L_q i_{sq}$$

(5)

$$v_{sq} = R_s i_{sq} + L_q \frac{di_{sq}}{dt} + \omega_e \left(L_d i_{sd} + \psi_f \right)$$

The electrical rotating speed of the generator defined by:

(6) $$\omega_e = p\omega_r$$

The electromagnetic torque is given by:

(7) $$T_{em} = \frac{p}{\omega_r}\left(i_q e_q\right) = p\psi_f i_q$$

The mechanical equation for the PMSG is expressed as:

(8) $$\frac{Jd\omega_r}{dt} = T_{em} - T_l - f\omega_r$$

Modelling of solar PV

Figure 3 shows, the PV cell is formed from a diode and a current source was connected antiparallel with a series resistance [9]. The PV system is based on solar energy, where PV cell is the most basic generation part in PV.

The relation of the current and voltage in the single-diode cell can be written as follows:

(9) $$i_{PV} = i_{ph} - i_0 \left(\exp\left(\frac{q\left(v_{PV} + R_{s\,\mathrm{mod}} i_{PV}\right)}{A_q KT} \right) - 1 \right)$$

In Figure 4, we notice that the increase in the short-circuit current is much greater than the increase in the open circuit voltage, because the short-circuit current is a linear function of the illumination and the open circuit voltage is a function logarithmic.

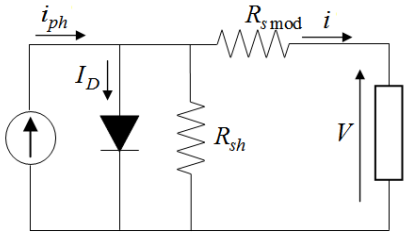

Fig 3. Equivalent circuit of PV cell

The Figure 5 shows the influence of irradiation on the power P which increases with increasing irradiance.

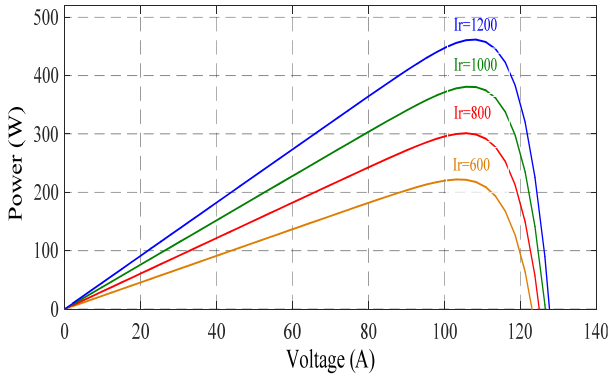

Fig 4. Voltage-Power curve of PV panel

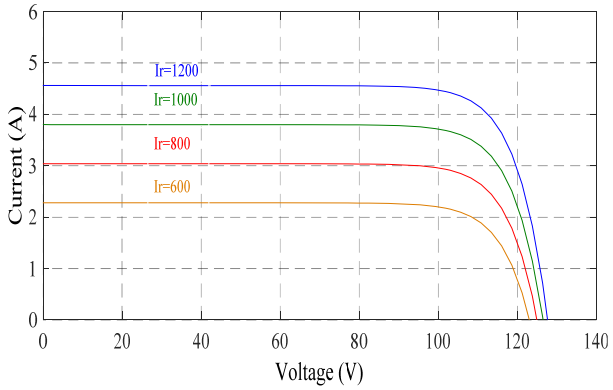

Fig 5. Voltage-current curve of PV panel

Solar Photovoltaic with MPPT Control

The variation of the charge requires the implementation of a DC / DC boost converter which makes it possible to increase the delivered solar voltage.

The configuration is shown in Fig. 6, which consists of a DC input voltage V_{in}, inductor L, switch *S*, diode *D* and capacitor *C* for filter [10].

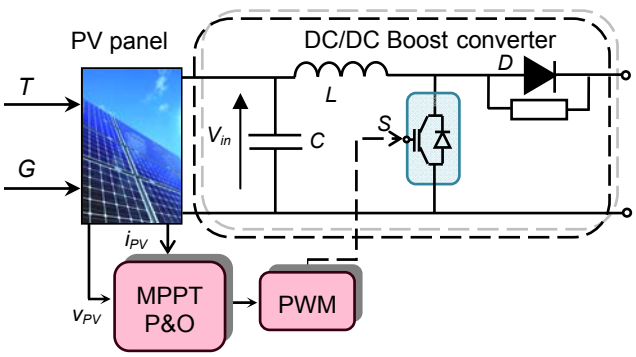

Fig. 6. DC/ DC Boost converter with MPPT control

The MPPT technique increases the efficiency of the solar panel. It is based on the application of the maximum power transfer theorem which says that the load will receive maximum power when the source impedance is equal to the load impedance.

The duty cycle of the DC/DC converter is controlled by the MPPT technical to extract the maximum power from the solar panel which results in the adaptation of the load impedance at the source [11].

Battery Modeling and Control

The equivalent scheme of the battery contains a voltage source which is the open circuit voltage, in series with an internal resistance as shown in Fig. 7.

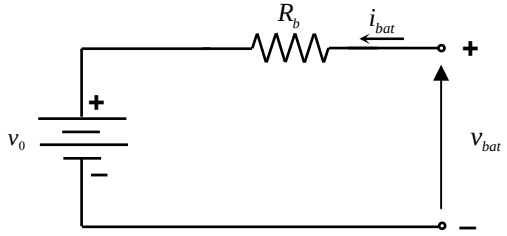

Fig. 7. The equivalent circuit of the battery

The output voltage of the battery is:

(10) $$v_{bat} = v_0 - R_b i_{bat}$$

The both v_{bat} and i_{bat} depend on the battery state of charge (*SOC*), temperature and internal resistance variations.

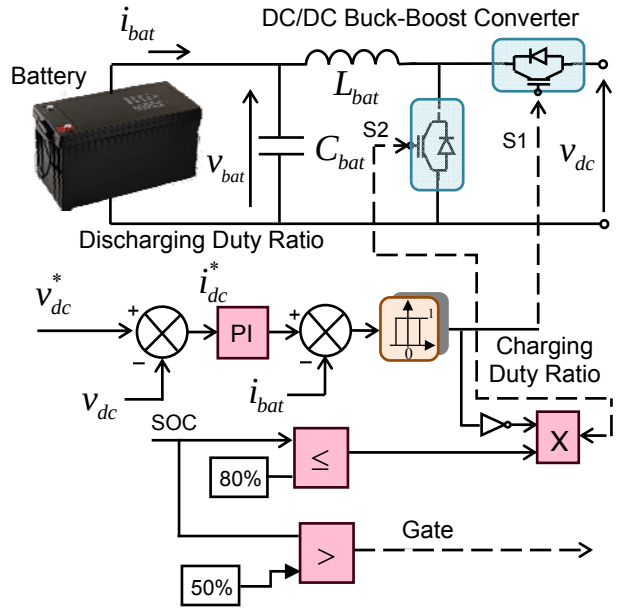

Fig. 8. The battery control

During the charging and discharging process, the state of charge (*SOC*) in terms of time (t) can be described by [12]:

(11)

$$SOC(t) = \begin{cases} SOC(t-\Delta t) + P_{bat} \cdot \dfrac{\eta_{ch}}{C_n . v_{dc}} . \Delta t \\ SOC(t-\Delta t) + P_{bat} \cdot \dfrac{1}{\eta_{dis} . C_n . v_{dc}} . \Delta t \end{cases}$$

At any time step Δt, the SOC must comply with the following constraints

(12) $$SOC_{\min} \le SOC(t) \le SOC_{\max}$$

The storage system is connected to the DC network via a bidirectional Buck/Boost DC/DC converter. In order to obtain the required power, it is necessary to control the current of the battery. Charge and discharge current limits and maximum *SOC* limits are also included in the model. Fig. 8 illustrates the principle of battery control [13].

The battery storage will operate in charging, discharging or floating modes depending on the energy requirements and these modes are managed according to the DC bus voltage at the battery storage point of coupling. Consequently, the battery storage is required to provide necessary DC voltage level under different operating modes of the grid and the AC load. When charging, switch S2 is activated and the converter works as a boost circuit; otherwise, when discharging, switch S1 is activated and the converter works as a buck circuit. When the voltage at the DC link is lower than the voltage reference, switch S1 is activated. Alternatively, when the voltage at the DC link is higher than the voltage reference, switch S2 is activated. The PV-wind-battery system response to transient variations is characterized by an inherent time constant. In such cases, capacitors along the DC grid can act as virtual inertia to supply the shortfall or absorb the surplus of energy [14, 15].

The DC-link power balance can be expressed by the following differential equation:

(13) $$v_{dc} i_{dc} = P_{PV} + P_W + P_{bat} - P_{load}$$

The power balance of the integrated hybrid generation system with energy storage is given by:

(14) $$v_{dc} i_{dc} = C v_{dc} \frac{dv_{dc}}{dt} = P_{PV} + P_W + P_{bat} - P_{load}$$

This equation is formulated by neglecting the losses in the power converters, the battery, the filtering inductors and the transformer as well as the harmonics due to the switching actions.

The main objective of the battery control is to maintain constant the voltage at the DC link. If the powers injected by the two DC/DC converters are assumed constant at any particular instant, the battery power guarantees adjustment of the capacitor voltage.

Five Levels Flying Capacitors Inverter

The flying capacitors inverter structure is characterized by a nested connection of the switching cells (Fig. 9) [16]. Each arm of the inverter consists of four cells. The circuit has been called the flying capacitor multi-level inverter (FCMLI) with independent capacitors clamping the device voltage to one capacitor voltage level. The operating principle of the converter is described in [17, 18].

System Configuration of the Proposed Multi-source Scheme

The Fig. 10 describes the multi-source scheme of solar-wind and battery connected to the power grid through a flying capacitor inverter and its control strategies.

The main objective of this study is to evaluate system operation based on desired criteria and to define a proper control algorithm and a dispatch strategy to extract the maximum available energy from the solar and wind sources. In order to achieve this goal, a model has been developed to evaluate the system operation. Energy demand is predicted for an emergency situation and a load profile is determined.

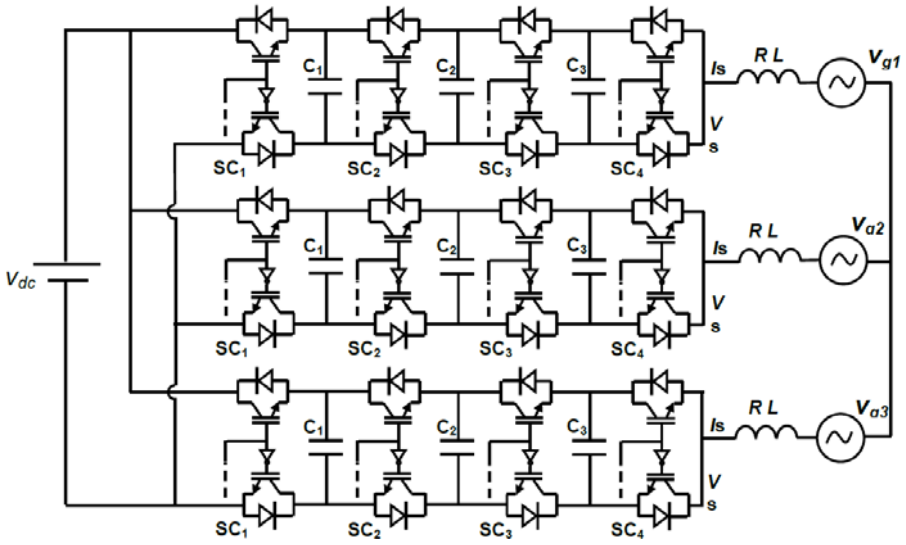

Fig. 9. Five level flying capacitors inverter

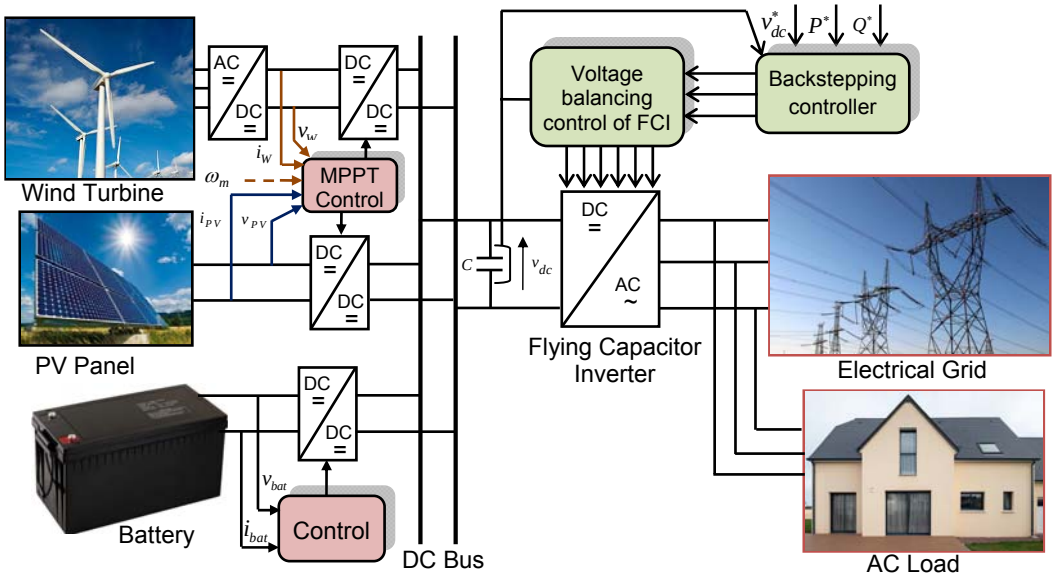

Fig. 10. Proposed configuration of multi-source system with battery connected to the power grid

Active and reactive Backstepping control

The backstepping control strategy is based on the representation of the looped systems in the form of Lyapunov order 1 subsystems. This is translated into the robustness against the perturbations and overall system stability [19].

The backstepping control is based on a multistep method, and at each stage, a virtual command is

generated to ensure that the system converges to its equilibrium state. The stabilization of each synthesis step is ensured by the Lyapunov functions.

Three-phase grid voltages are represented by the following equations:

$$\begin{cases} v_{ga} = v_{\max}\cos(\omega t) \\ v_{gb} = v_{\max}\cos\left(\omega t - \dfrac{2\pi}{3}\right) \\ v_{gc} = v_{\max}\cos\left(\omega t - \dfrac{2\pi}{3}\right) \end{cases} \tag{15}$$

The synchronization of current with the mains voltages and the DC bus voltage adjustment are provided by the mains side converter, the backstepping control is used to control the active and reactive power supplied to the mains [20].

The voltages in the d-q frame of reference are represented by the following equations:

$$\begin{cases} v_{gd} = v_{id} - R_g i_{gd} - L_g \dfrac{di_{gd}}{dt} + \omega_g L_g i_{gq} \\ v_{gq} = v_{iq} - R_g i_{gq} - L_g \dfrac{di_{gq}}{dt} - \omega_g L_g i_{gd} \end{cases} \tag{16}$$

The grid currents in the d-q frame of reference can be expressed as follows:

$$\begin{cases} \dfrac{di_{gd}}{dt} = \dfrac{v_{id}}{L_g} - \dfrac{R_g}{L_g} i_{gd} + \omega_g i_{gq} - \dfrac{v_{gd}}{L_g} \\ \dfrac{di_{gq}}{dt} = \dfrac{v_{iq}}{L_g} - \dfrac{R_g}{L_g} i_{gq} - \omega_g i_{gd} - \dfrac{v_{gq}}{L_g} \end{cases} \tag{17}$$

The module of the total voltage and current of the grid is established by:

$$\begin{aligned} \left|v_g\right| &= \sqrt{\left(v_{gd}\right)^2+\left(v_{gq}\right)^2} \\ \left|i_g\right| &= \sqrt{\left(i_{gd}\right)^2+\left(i_{gq}\right)^2} \end{aligned} \tag{18}$$

The active and reactive powers in the d-q reference frame are given by:

$$\begin{aligned} P_g &= \frac{3}{2}\left(v_{gd}i_{gd}\right)=\frac{3}{2}\left(\left|v_g\right|i_{gd}\right) \\ Q_g &= \frac{3}{2}\left(-v_{gd}i_{gq}\right)=-\frac{3}{2}\left(\left|v_g\right|i_{gq}\right) \end{aligned} \tag{19}$$

The control strategy applied to the GSC is based on making:

$$\begin{aligned} v_{gq} &= 0 \\ v_{gd} &= \left|v_g\right| \end{aligned} \tag{20}$$

The powers equations become:

$$\begin{aligned} P_g &= \frac{3}{2}\left(v_{gd}i_{gd}+v_{gq}i_{gq}\right) \\ Q_g &= \frac{3}{2}\left(v_{gq}i_{gd}-v_{gd}i_{gq}\right) \end{aligned} \tag{21}$$

The active and reactive powers dynamic is directly related to the components of the current.

Design of the Backstepping controller

The errors of the direct and quadrature grid current are defined by the following expressions [21]:

$$\begin{cases} e_{gd} = i_{gd}^{*}-i_{gd} \\ e_{gq} = i_{gq}^{*}-i_{gq} \end{cases} \tag{22}$$

The error dynamics will be calculated as follows:

$$\begin{cases} \dot{e}_{gd} = -\dot{i}_{gd} \\ \dot{e}_{gq} = -\dot{i}_{gq} \end{cases} \tag{23}$$

The Lyapunov function according to the computed errors of the grid currents is determined as follows:

$$V = \frac{1}{2}\left(e_{gd}^2+e_{gq}^2\right) \tag{24}$$

The Lyapunov function dynamics can be derived as follows:

(25)

$$\begin{aligned} \dot{V} = &-K_{gd}e_{gd}^2-K_{gq}e_{gq}^2 \\ &+e_{gd}\left(\frac{v_{id}}{L_g}-\frac{R_g}{L_g}i_{gd}+\omega_g i_{gq}-\frac{v_{gd}}{L_g}+K_{gd}e_{gd}\right) \\ &+e_{gq}\left(\frac{v_{iq}}{L_g}-\frac{R_g}{L_g}i_{gq}-\omega_g i_{gd}-\frac{v_{gq}}{L_g}+K_{gq}e_{gq}\right) \end{aligned}$$

To obtain stability through this Lyapunov function, a positive value must be selected for the gains K_{gd} and K_{gq}, and the derivative function must be negative. Consequently, we have to choose the reference voltages as follows:

$$\begin{cases} v_{id}^{*} = R_g i_{gd}-\omega_g L_g i_{gq}-L_g K_{gd}e_{gd}+v_{gd} \\ v_{iq}^{*} = R_g i_{gq}+\omega_g L_g i_{gd}-L_g K_{gq}e_{gq}+v_{gq} \end{cases} \tag{26}$$

Equations (21) provide the direct and quadrature current of the references as expressed by the following relationships:

The i_{gq}^{*} current can be obtained from the following relation:

$$i_{gq}^{*} = -\frac{2Q_g^{*}}{3v_{gq}} \tag{27}$$

If the reference reactive power is forced to be zero $Q_g^{*}=0$, the system will operate with a unity power factor.

The calculation of the direct reference current igd-ref is obtained through the DC bus voltage regulation. The DC link voltage is regulated at the reference value v_{dc}^{*}, and if the converter losses are neglected, the transferred active power will be defined as follows:

$$P_g = \frac{3}{2}\left(v_{gd}i_{gd}\right)=v_{dc}i_{dc} \tag{28}$$

Thus, the i_{gd}^{*} current is obtained from (Equation 28):

$$i_{gd}^{*} = \frac{2P_g^{*}}{3v_{gd}} \tag{29}$$

The backstepping control structure for the GSC and the DC-link voltage control is shown in Fig. 11.

To control the DC bus voltage VC, a regulator must be implemented to maintain this voltage constant regardless of the current flow rate on the capacitor. The DC bus equation can be written as follows [22]:

$$P_c = cv_{dc}\frac{dv_{dc}}{dt}=P_g-P_r \tag{30}$$

To control the dc voltage, we control the P_c in the capacitor by adjusting the power P_g using a conventionnal PI controller.

Capacitors Voltage Balancing Control of Flying Inverter

Capacitor voltage balancing control due to factors such as dynamic output process, parameter difference, modulation dead zone or calculation deviation and the practical voltage on capacitors may vary from the reference voltage with an open loop control.

The unbalanced capacitor voltages increase the possible voltage constraint of the switching devices and affect the harmonic characteristic of the output current. As a result, a capacitor voltage closed-loop regulation is necessary. Since the topology capacitors can be classified as DC-bus capacitors and flying capacitors, the regulation process can also be divided into two parts. The first part is designed to stabilize the DC-bus capacitor voltages. The second part is designed to stabilize all flying capacitor voltages by regulating relative flying capacitor currents [21].

The complete voltage balancing control of the FC inverter is shown in Fig. 12.

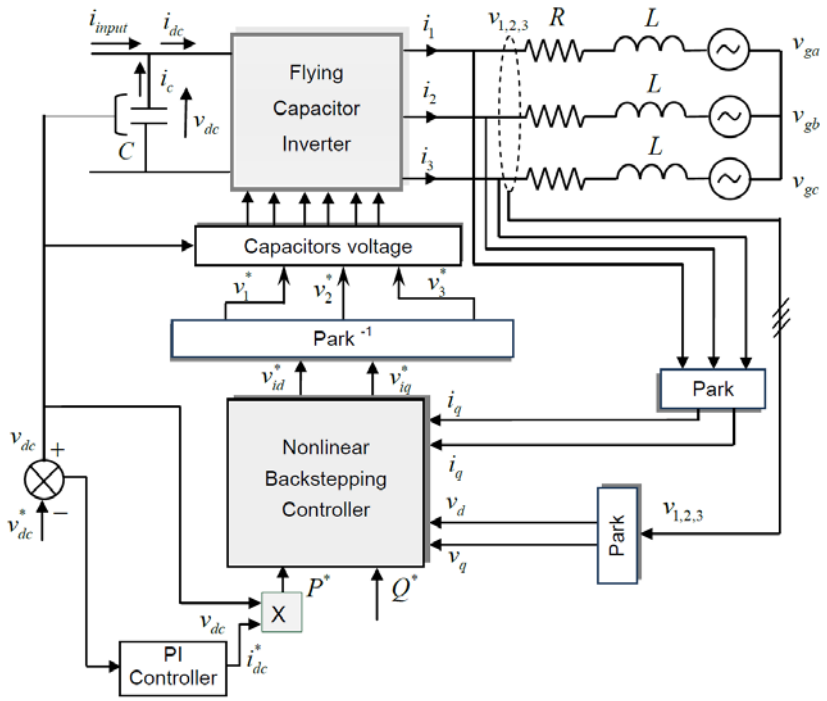

Fig. 11. Block diagram of nonlinear backstepping control of current for active and reactive power

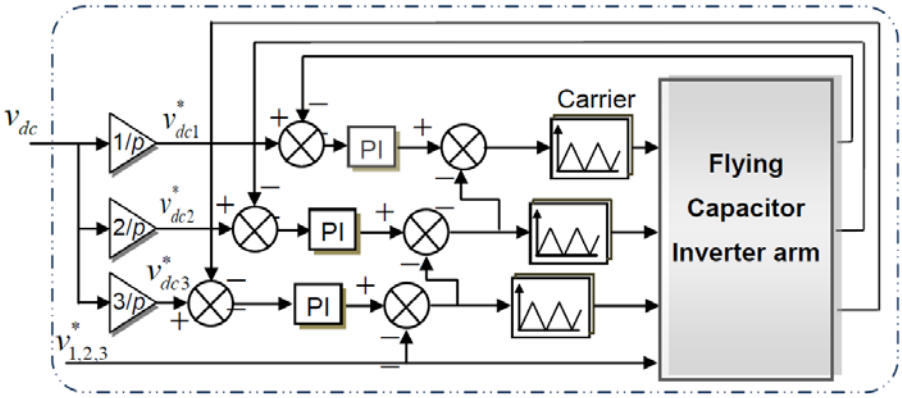

Fig. 12. Structure of capacitor voltage balancing control of flying inverter (p=4)

Simulation Results and Discussions

The simulations carried out to check the validity of the proposed scheme used nonlinear backstepping control to regulate the DC voltage and the current of a five level flying capacitor inverter connected to the multi-sources (PV-wind turbine-battery) system integrated with an AC load and a grid.

To verify the effectiveness and robustness of the proposed controller, the simulation is carried out in Matlab/Simulink using SimPowerSystems models. The proposed system parameters are listed in Table 2, 3, 4 and 5.

The amount of power generated/supplied by the PV array depends on the variable solar irradiation G = [600, 1000, 800] W/m^2 at the time t= [0, 2, 3.5, 8] s respectively and the temperature T = 293 K. The proposed system is operated in six possible operating modes depending on the variable load. The system performance for this situation is shown in Figs. 13 to 20.

Fig. 13 describe the PV proprieties. The power and the current, voltage and SOC are shown in Fig. 14 and 15 respectively. Fig. 14 shows the power distribution (load, PV, wind and battery). Fig. 16 show the performance of the wind turbine.

The figure 17 display the performance of the current and the voltage delivered by the wind turbine and the DC boost assembly. It should be noted that these quantities increase at t = 4 sec. This increase is due to the variation of the wind profile

Initially, between t = 0 s and t = 3 s, the load is varied from 0 kW to 7 kW. The grid can supply the power to the load and the PV charges the battery storage system. At t = 1 second, the grid is disconnected and the load which is always set at 7 kW is supplied simultaneously by the PV and the battery. We notice at t = 2 s, the battery begins to discharge, the PV reacts to make the compensation. Then, the load is increased from 7 kW to 10 kW between t = 1 s and 3 s. As a result shown, with this variation, the PV remains constant. However, it is the battery which passes to the compensation which corresponds to satisfy the new power demand.

Between t = 3 and 4 seconds, the demand increases to 10 kW, in this interval, the three sources intervene to ensure this demand.

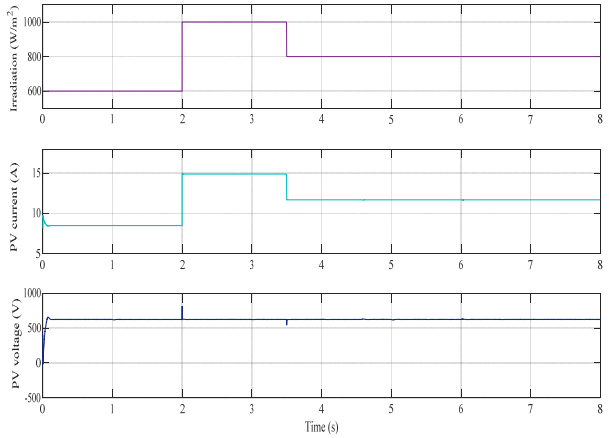

Fig. 13. PV generator output voltage and current under varying irradiation levels

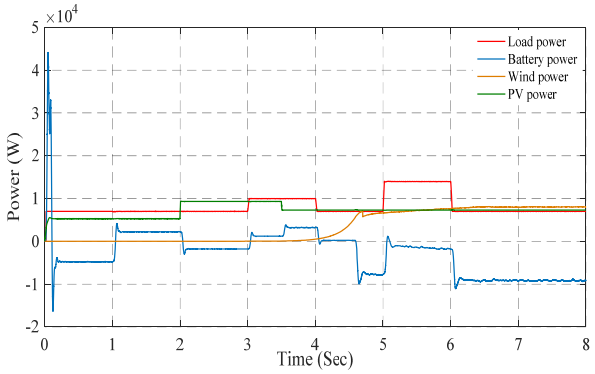

Fig. 14. Power generation of the hybrid system on grid under varying load demand profile AC load

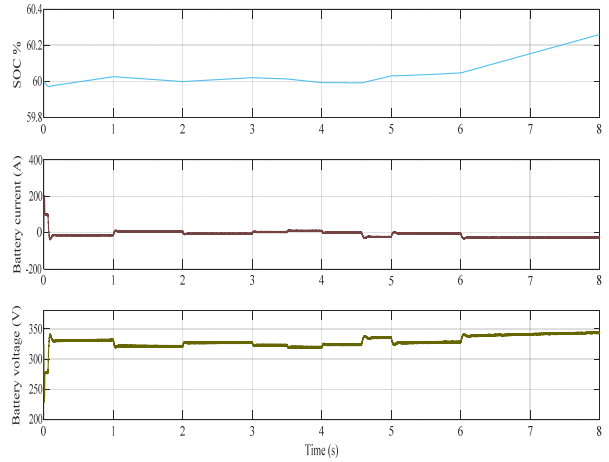

Fig. 15. Global state of charge (SOC), voltage and current battery

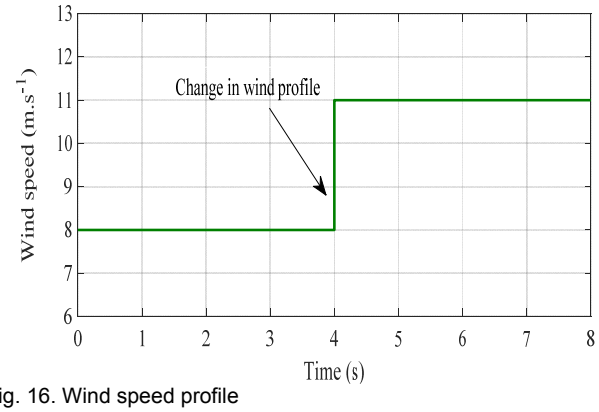

Fig. 16. Wind speed profile

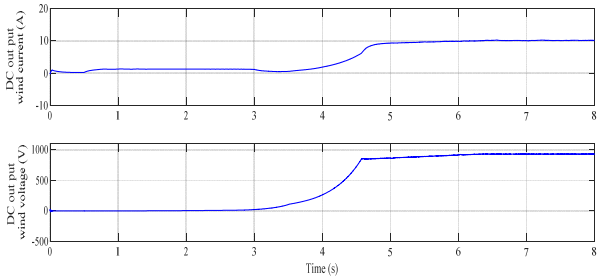

Fig. 17. DC Output wind current and voltage

The load decreases to 7 kw again between t = 4 and 5 seconds, the power of the battery remains constant instantaneously at t = 4.6 s in this period then it charges the rest of the time, while the wind turbine which produces energy.

Between t = 5 s and 6 s, the wind turbine continues to generate energy, the PV remains at constant production and the battery is in the state of charge and all this following an increase in demand to 14 kW.

Finally, between t = 6 s and t = 8 s, the load is varied from 14 kW to 7 kW. The wind turbine also supplies energy to the load to ensure stability between the generated power by the PV / battery storage system and the load demand. In this study, as mentioned earlier, the battery storage has two essential roles in the multi-sources system.

The Fig. 18 and 19 respectively show the current and the voltage of the load with their zoom, they are purely sinusoidal which shows the efficiency of the control strategy applied to the converter which gives a better quality of energy to the load.

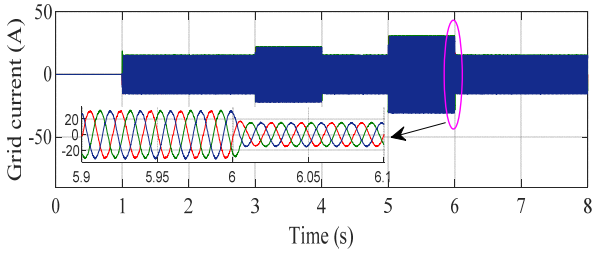

Fig. 18. Current of output inverter and its zoom

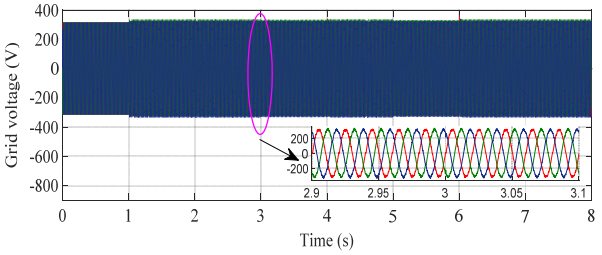

Fig. 19. Voltage of output inverter and its zoom

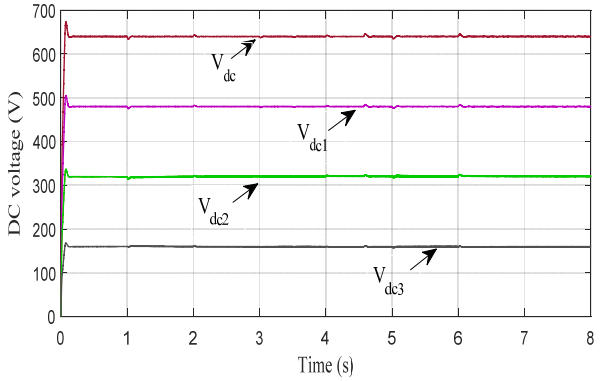

Fig. 20. DC voltage performance in the DC link

The first is to supply energy to the load to ensure stability between demand and generation while the second is to ensure the stability of the voltage against DC bus voltage drop (Fig. 20). From these results, it can be concluded the power management algorithm is able to achieve good control and balance between the power required by the load and multi-sources system generation under the simulated operating conditions.

Extensive simulations under different working conditions are performed for the considered hybrid dynamic process. The achieved results indicate that the proposed methodology is effective to accurately describe the hybrid power generation dynamic system.

Conclusions

In this work a multi-sources energy system PV/wind turbine and battery have been presented. Dynamic modeling and simulations of the hybrid system is proposed using Matlab/Simulink. We developed and tested this hybrid energy system and its supervision-control system. The combination of the photovoltaic generator, the wind turbine and the battery allows satisfying the load request. The conversion of the output of solar and wind systems into alternating current output is ensured by the use of a five-level flying capacitor inverter. Circuit Breaker is used to connect and disconnect an additional load in the given time. To meet load requirements, this multi-source system is controlled to provide maximum output power under all operating conditions.

The aim of the backstepping control strategy is to maximize energy extraction from wind and solar energy, to improve battery performance and to use the excess energy for battery charging and optimization of plant operation.

These results show the efficiency of the management and the control used for this study. We can also propose as future works and perspectives of used in this hybrid system a PV, wind, battery all associated with a supercapacitor. These proposed approaches can be implemented easily with DSP or Dspace platform.

APPENDIX

Table 1. PMSG parameters

Components	Rating values
Rated power	8.5 kW
Type of Generator	PMSG
Rated Speed	1800
Number of poles	10

Table 2 PV Parameters

Components	Rating values
Peak Power	200 W
Peak Voltage	660 V
Peak current	7.52 A
Open Circuit Voltage	33.2 V
Short Circuit Current	8.36 A

Table 3 Battery and AC Load Parameters

Components	Rating values
Load 1, 2, 3, 4, 5 (R)	7 kW, 10 kW, 7 kW, 14 kW, 7 kW
Battery type	Nickel Metal hydride
Nominal voltage	300 V
Capacity rating	6.5 AH

Table 4 DC/DC Bi-converter and five level flying capacitor Inverter

Components	Rating values
C_1=C_2=C_3	450 µF
Dc link Voltage	640 V
Frequency	50 Hz
Converter Inductor	5 mH
DC link Voltage	640 V
Converter Capacitor	2.2 mF

Table 5 Wind turbine parameters

Components	Rating values
C1=C2	2.2 mF
Dc link Voltage	640 V
Frequency	50 Hz
Converter Inductor	5 mH
DC link Voltage	640 V
Converter Capacitor	2.2 mF

Nomenclature:

v_{gd} , v_{gq} - Grid peak voltages in dq-frame [V]
i_{gd} , i_{gq} Grid peak currents in dq-frame
v_{sd} , v_{sq} are the d, q components of the stator voltage
v_{id} , v_{iq} Voltage inverter d, q components [V]
v_{ga} , v_{gb} Three phase grid voltages [V]
v_{max} The phase voltage amplitude
ω The angular frequency
v_{PV} Photovoltaic system output voltage [V]
v_{bat} The voltage battery [V]
v_0 The internal voltage of the battery [V]
i_{bat} The current battery [A]
P_{bat} The power battery [W]
P_{PV} Photovoltaic power [W]
P_{load} Load power [W]
i_{sd} , i_{sq} The d, q components of the stator current
i_{PV} Photovoltaic current [A]
i_{ph} Photocurrent of a solar PV cell generated due to solar irradiation [A]
i_0 Diode's Reverse saturation current [A]
Ψ_f The permanent magnetic flux [Wb]
q Charge of electrons [C]
T Absolute temperature [°K]
K Boltzmann constant [1.3806503*10^{-23}J/K]
R_s The stator resistance
R_g The resistance of the intermediate filter between the GSC and the grid
L_g The reactance of the intermediate filter between the GSC and the grid
A_a Curve fitting or diode ideality constant
R_{smod} Series resistance [Ω]
L_d, L_q The d, q components of the stator inductance [mH]
ω_e The electrical rotating speed of the generator
ω_r The mechanical rotational speed of the generator
R_b The internal resistance of battery [Ω]
η_{ch}, η_{dis} Are respectively the battery efficiencies during charging and discharging phase
C_n The nominal capacity of the battery [mF]
L_{gd}, L_{gq} Input filter inductance d, q components [mH]
Δt Time variation [sec]
v_{dc} Dc bus voltage [V]
v^*_{dc} Reference Dc bus voltage [V]
i_{dc} Dc bus current [A]
C DC link capacitor [mF]
R_b The battery resistance [Ω]
P_g Grid active power [kW]
P^*_g Grid active power reference [kW]
P_c The power in capacitor
P_g Grid active power
P_r The active power at rotor side converter
P_m The mechanical power
P The number of pole pairs in a generator
Q_g Grid reactive power [kVAR]
Q^*_g Grid reactive power reference [kVAR]
T_w The torque wind [Nm]
T_{mec} The mechanical torque [Nm]
T_l The load torque [Nm]
J The motor inertia [Kg.m^2]
f Viscous friction coefficient [N.m/rad/sec]
φg Grid power factor angle (angle between grid voltage and current) [degree]

ρ	The air density of [kg.m^{-3}]
A	The rotor swept area [m^2]
C_p	The power coefficient
v_W	The wind speed apstream of the rotor [m.s^{-1}]
P_w	The power extracted from wind [W]
R_r	The rotor radius
ω_W	The angular vilocity of the rotor [rad/s]
ω_g	The grid angular pulsation
λ	The tip speed ratio
β	The pitch angle
AC	Alternatif Current
DC	Direct Current
DSP	Digital Signal Processor
FCM	Flaying Capacitor Multi-Level Inverter
GSC	Grid Side Converter
MPPT	Maximum Power Point Tarcking
PI	Proportionnal Intergal
PMS	Power Managment System
PMSG	Permanent Magnet Synchronous Generator
Pu	Pert Unit
PV	Photovoltaic
RSC	Rotor Side Converter
SOC	State Of Charge
WT	Wind Turbine

Authors *Bachir Boumediene, Laboratory of Energy and Computer Engineering L2GEGI, Department of Electrical Engineering, Faculty of Applied Sciences, University of Tiaret, BP 78 Size Zarroura, Tiaret 14000, Algeria, bachir.boumediene@univ-tiaret.dz*
Attalah Smaili, Laboratory of Energy and Computer Engineering L2GEGI, Department of Electrical Engineering, Faculty of Applied Sciences, University of Tiaret, BP 78 Size Zarroura, Tiaret 14000, Algeria, attalah.smaili@univ-tiaret.dz
Tayeb Allaoui, Laboratory of Energy and Computer Engineering L2GEGI, Department of Electrical Engineering, Faculty of Applied Sciences, University of Tiaret, BP 78 Size Zarroura, Tiaret 14000, Algeria, tayeb.allaoui@univ-tiaret.dz
Abderrahmane Berkani, Laboratory of Energy and Computer Engineering L2GEGI, Department of Electrical Engineering, Faculty of Applied Sciences, University of Tiaret, BP 78 Size Zarroura, Tiaret 14000, Algeria, abderrahmane.berkani@univ-tiaret.dz
Fabrizio Marignetti, Dipartimento di Automazione Università degli Studi di Cassino*, Italy, marignetti@unicas.it*

REFERENCES

[1] Koulali M., Mankour M., Negadi K., Mezouar A., Energy management of hybrid power system PV Wind and battery based three level converters, Tecnica Italiana-Italian Journal of Engineering Science, Vol 63, No 2-4, pp 297-304, https://doi.org/10.18280/ti-ijes.632-426.
[2] Belabbas B., Allaoui T., Tadjine M., Denai M., Power management and control strategies for off-grid hybrid power systems with renewable energies and storage, Energy Syst (2019) 10:355–384, https://doi.org/10.1007/s12667-017-0251-y.
[3] Allani M.Y., Tadeo F., Mezghanni D., Mami A., Modelling and control of a grid-connected hybrid photovoltaic/wind/battery system coupled to an AC load, IJCSNS International Journal of Computer Science and Network Security, Vol 19 No 5, May 2019.
[4] Kouadria S., Berkouk E., Messlem Y., Denaı M. Improved control strategy of DFIG-based wind turbines using direct torque and direct power control techniques, Journal of Renewable and Sustainable Energy 10, 043306 (2018), https://doi.org/10.1063/1.5023739.
[5] Shafiyi M.A., Khederzadeh M., Meisam Sadeghi., Khani S., A Grid-connected PV Power Supply based on Flying Capacitor multicell converter with modified MPPT based Control for Active Power Filtering, Second Iranian Conference on Renewable Energy and Distributed Generation, 2012.
[6] Fan B., Wang K., Li Y., Xu L., Zheng Z., Capacitor Voltage Balancing Control of a Flying Capacitor Based n-level DC-DC Converter, 17th European Conference on Power Electronics and Applications (EPE'15 ECCE-Europe), IEEE, 2015.
[7] Eduardo Giraldo., Alejandro Garces., An Adaptive Control Strategy for a Wind Energy Conversion System Based on PWM-CSC and PMSG, IEEE Transactions On Power Systems, Vol. 29, No. 3, May 2014.
[8] Nabil Karami , Nazih Moubayed , Rachid Outbib ,Energy management for a PEMFC–PV hybrid system, http://dx.doi.org/10.1016/j.enconman.2014.02.070, Energy Conversion and Management 82 (2014) 154–168.
[9] El Magri A., Giri F., El Fadili A., Dugard L., Adaptive Nonlinear Control of Wind Energy Conversion System with PMS Generator, 11th IFAC International Workshop on Adaptation and Learning in Control and Signal Processing July 3-5 2013, Caen, France
[10] Sivasankari P., Padmini S., Chandran Ilambirai R., Modelling control power management of grid connected hybrid PV battery diesel system, AIP Conference Proceedings 2112, 020103 (2019), https://doi.org/10.1063/1.5112288.
[11] Tazay A.F, Ibrahim A.M.A, Noureldeen O, Hamdan I, Modeling, Control, and Performance Evaluation of Grid-Tied Hybrid PV/Wind Power Generation System: Case Study of Gabel El-Zeit Region, Egypt, Digital Object Identifier 10.1109/ACCESS.2020.2993919, IEEE Access, May 2020.
[12] Mosaad M.I., Osama abed el-Raouf M., Al-Ahmar M.A., Banakher F.A, Battery Charge Management for Hybrid PV/Wind/Fuel Cell with Storage Battery, Energy Procedia 162, 117-126 (2019).
[13] R. Araria, K. Negadi, M. Boudiaf, F. Marignetti, Non-Linear Control of DC-DC Converters for Batery Power Management in Electric Vehicle Application, Przeglad Elektrotechniczny, doi:10.15199/48.2020.03.20.
[14] Miñambres-Marcos V.M., Guerrero-Martínez M.Á., Barrero-González F., Milanés-Montero M.I., A Grid Connected Photovoltaic Inverter with Battery-Supercapacitor Hybrid Energy Storage, Sensors 2017, 17, 1856, doi:10.3390/s17081856, Published: 11 August 2017.
[15] Ameur K., Hadjaissa A., Cheknane A., Essounbouli N., DC-Bus Voltage Control Based on Power Flow Management Using Direct Sliding Mode Control for Standalone Photovoltaic Systems, Electric Power Components and Systems, March 2017.
[16] Berkani A., Negadi K., Allaoui T., Mezouar A., Denai M., Imposed Switching Frequency Direct Torque Control of Induction Machine using Five Level Flying Capacitors Inverter, European Journal of Electrical Engineering, Vol. 21, No. 2, April, 2019, pp. 241-248.
[17] Kotturu J., Kothuru S., Desai R., Performance Evaluation of Flying Capacitor Multilevel Inverter Based Induction Motor Drive, International Journal of Engineering Research & Technology (IJERT), Vol 4 Issue 01, January 2015.
[18] Dhivya K., Kumar.V M., Babu E., A Novel Flying Capacitor Multilevel Inverter With Stable Output Voltage, International Journal of Advanced Research and Publications.
[19] El Mourabit Y., Derouich A., El Ghzizal A., El Ouanjli N., Zamzoum O., Nonlinear backstepping control for PMSG wind turbine used on the real wind profile of the Dakhla-Morocco city, Int Trans Electr Energ Syst. 2020;e12297, DOI: 10.1002/2050-7038.12297, 2020 John Wiley & Sons, Ltd.
[20] Boudali A., Negadi K., Berkani A., Boudiaf M., Marignetti F., Fuzzy logic control of DFIG small hydropower plant connected to the electrical grid. Tecnica Italiana-Italian Journal of Engineering Science, Vol. 64, No. 2-4, pp. 303-311. https://doi.org/10.18280/ti-ijes, 642-427.
[21] El Azzaoui M., Mahmoudi H., Boudaraia K., Backstepping Control ofWind and Photovoltaic Hybrid Renewable Energy System, International Journal of Power Electronics and Drive Systems (IJPEDS) Vol. 7, No. 3, September 2016, pp. 677 – 686 ISSN: 2088-8694.
[22] Bechouat M., Sedraoui M., Soufi Y., Yousfi L., Borni A., Particle S.K., Swarm Optimization Backstepping Controller for a Grid-Connected PV/Wind Hybrid System, Journal of Engineering Science and Technology Review Volume 10, Issue 1, 2017, Pages 91-99.
[23] Boujmil M.H., Badis A., Mansouri M.N., Nonlinear Robust Backstepping Control for Three-Phase Grid-Connected PV Systems, Hindawi Mathematical Problems in Engineering Volume 2018, Article ID 3824628, 13 pages https://doi.org/10.1155/2018/3824628